**Supporting Information**

# Layer-by-Layer Processed Efficient Semi-Transparent Organic Solar Cells Enabled by Trace-Doped Acceptor Layer Strategy

Dan Wang[1], Fenghua Zhang[1], Yang Liu[1], Yang Zhang[1], Mandi Li[1], Jun Zhou[1], Yao-hui Zhu[1], Ge Song[2]*, Xiong Li[1]*, Denghui Xu[1]*

[1]*Department of Physics, Beijing Technology and Business University, Beijing, 100048, China*

[2]*Clinical Laboratory Department, The Affiliated Hospital of Liaoning University of Traditional Chinese Medicine, Shenyang, Liaoning, 110000, China*

Corresponding authors:

E-mail: songge0109@163.com (G. Song), lixiong@btbu.edu.cn(X. Li), xudh@btbu.edu.cn (D. Xu)

## Experimental section

### 1. Materials

All materials and solvents were employed as received, without further purification unless otherwise specified. The polymer donor PM6, small molecule acceptor L8-BO, and electron transport layer PDINN were sourced from Solarmer Material Inc. The hole transport layer PEDOT:PSS (Clevios P Al4083) was procured from Heraeus. 1,8-Diiodooctane (DIO) was obtained from J&K Scientific Ltd. For electrode evaporation, high-purity gold and silver (≥99.99%) were used.

### 2. Solution preparation

The PM6 layer solution was formulated by dissolving the polymer in chloroform to a concentration of 8 mg/ml and subsequently stirring the mixture at 50 °C for 2 hours. For the acceptor layer, L8-BO was dissolved in chloroform to achieve an 8 mg/ml concentration. PM6 and L8-BO with different mass ratios (0 wt%, 5 wt%, 10 wt%, 15 wt% PM6) were mixed and dissolved in chlorobenzene (CF) to achieve a total concentration of 8 mg/ml. Subsequently, 0.3 vol% of 1,8-diiodooctane (DIO) was added as a solvent additive. The resulting solution was stirred at 50 °C for 2 hours. All the active layer solutions are stirred in a high-purity nitrogen-filled glove box. The cathode buffer layer solution was prepared by dissolving PDINN in methanol to a concentration of 1.5 mg/ml.

### 3. Device fabrication

To enhance the transparency of the devices in the visible region, the thickness of the PM6 layer was optimized. During the experiments, the film thickness was controlled by adjusting the rotation speed of the spin coater. Figure 4.3(a) shows the PM6 film thicknesses at different rotation speeds. To investigate the effect of donor layer thickness on semi-transparent devices, conventional opaque devices with varying PM6 thicknesses were fabricated, and the device structure is ITO/PEDOT:PSS/PM6/L8-BO/PDINN/Ag(15 nm). The J-V characteristics were measured as shown in Figure 4.3(b). The corresponding photovoltaic parameters are summarized in Table S5. The opaque device exhibited optimal electrical performance at a PM6 spin-coating speed of 4000 rpm. However, considering the transparency requirement, a speed of 5000 rpm was selected as the optimal condition for the donor layer, as the electrical performance showed no significant degradation while yielding a thinner film.

The ST-OSCs were fabricated using a standard architecture consisting of ITO glass/PEDOT:PSS/PM6/L8-BO:x%PM6/PDINN/Au(1nm)/Ag(15nm). The ITO-coated glass substrates were subjected to a cleaning protocol involving two 30-minute detergent washes, followed by two 15-minute deionized water rinses to eliminate impurities and detergent residue. Finally, they were cleaned twice with anhydrous ethanol at room temperature to ensure substrate cleanliness. Prior to use, the substrates were treated with ultraviolet-ozone for 8 minutes. A 30-nm-thick PEDOT:PSS layer was initially spin-coated onto the ITO substrates at 3000 rpm for 40 seconds, followed by annealing at 150 °C for 30 minutes in an ambient atmosphere. Subsequently, the substrates were transferred into a glovebox filled with high-purity nitrogen gas, where the active layers were spin-coated. The PM6 layers were prepared by spin-coating the donor layer solutions at 5000 rpm for 30 seconds onto the PEDOT:PSS layer. The L8-BO:PM6 layer was made by spin-coating the L8-BO:PM6 solutions at 6000 rpm for 30 seconds onto the PM6 layers. L8-BO:PM6 solutions were made by PM6 and L8-BO with different mass ratios (0 wt%, 5 wt%, 10 wt%, 15 wt% PM6) that were mixed and dissolved in chlorobenzene (CF) to achieve a total concentration of 8 mg/ml. Subsequently, 0.3 vol% of 1,8-diiodooctane (DIO) was added as a solvent additive. The resulting solution was stirred at 50 °C for 2 hours prior to use. After deposition, the LBL layers were thermally annealed at 85 °C for 5 minutes in an $N_2$-filled glovebox. Subsequently, a thin layer (5 nm) of PDINN solution was spin cast on the top of the

active layer. Finally, 1 nm Au layer and 15 nm Ag layer were sequentially deposited by vacuum evaporation deposition under a vacuum condition of $3\times10^{-4}$ Pa. The devices were measured through a mask with an area of 0.045 $cm^2$.

**4. Measurements and Characterizations**

The UV-vis absorption spectra and the transmittance curves of the devices were analyzed using a UV-vis spectrophotometer (Hatachi-U3900H). The current density-voltage (*J-V*) characteristics were meticulously measured using a Keithley 2400 digital source meter, under standardized illumination of 100 mW/cm² provided by an AM 1.5 sunlight simulator (San-Ei Electric). The light intensity of the AM 1.5 G solar simulator was precisely calibrated with a standard silicon solar cell, ensuring accurate and reliable data acquisition. The external quantum efficiency (EQE) was measured using a solar cell QE/IPCE measurement system (Zolix solar cell scan100). Transient photovoltage (TPV), transient photocurrent (TPC), charge extraction (CE), photo-induced charge extraction under linearly increasing voltage (Photo-CELIV), and the dependence of $V_{OC}$ and $J_{SC}$ on light intensity were all comprehensively measured and analyzed using the advanced Paios system (FLUXiM AG, Switzerland). The morphology was analyzed using Bruker-Fast scan ultrafast DI atomic force microscope with soft-tapping mode. The thickness of each functional layer was measured by a Dektak XT (Dektak XT, Bruker Corporation) step meter. The GIWAXS data acquisition for the sample was performed at the BL16B1 beamline at the Shanghai Synchrotron Radiation Facility. The monochromatic of the light source was 1.164 Å.

The average visible transmittance (AVT) is determined by integrating the transmission spectrum and the AM 1.5G photon flux, with the calculation weighted by the photopic response of the human eye:

$$AVT = \frac{\int T(\lambda)\cdot V(\lambda)\cdot \mathrm{AM1.5}G(\lambda)d\lambda}{\int V(\lambda)\cdot \mathrm{AM1.5}G(\lambda)d\lambda}$$

where $\lambda$ is the visible region wavelength (380 nm-740 nm), $T(\lambda)$ is the transmission spectrum, $V(\lambda)$ is the human eye photopic response.

The contact angle images were obtained using a surface contact angle tester (XG-CAM, XYCXIE). The contact angles of pure PM6, L8-BO film and their blend films of PM6/L8-BO, PM6/L8-BO:5 wt% PM6, PM6/L8-BO:10 wt% PM6, and PM6/L8-BO:15 wt% PM6 were measured using water ($H_2O$) and ethylene glycol (EG) as the testing liquids, respectively.

**Reference**


[1] J. Jing, et al., Adv. Energy Mater. 12 (20) (2022) 2200453.

[2] H. I. Jeong, et al., Adv. Energy Mater. 11 (47) (2021) 2102397.

[3] W. Liu, et al., Adv. Mater. 34 (18) (2022) 2200337.

[4] T. Jiang, et al., Mater. Today Energy. 21 (2021) 100807.

[5] X. Huang, et al., J. Mater. Chem. A. 9 (9) (2021) 5711.

[6] Y. Xie, et al., Adv. Funct. Mater. 30 (28) (2020) 2002181.

[7] Y. Li, et al., Proc. Natl. Acad. Sci. 117 (35) (2020) 21147.

[8] X. Huang, et al., Adv. Funct. Mater. 32 (5) (2022) 2108634.

[9] Z. Hu, et al., Sci. Bull. 65 (2) (2020) 131.

[10] M. Bates, et al., Sol. RRL. 7 (10) (2023) 2200962.

[11] C. Xu, et al., Adv. Funct. Mater. 31 (52) (2021) 2107934.

[12] S. J. Jeon, et al., Small. 19 (38) (2023) 2301803.

[13] H. C. Wang, et al., Adv. Energy Mater. 11 (13) (2021) 2003576.

[14] H. Tang, et al., Org. Electron. 93 (2021) 106140.

[15] Q. Wei, et al., J. Mater. Chem. C. 10 (15) (2022) 5887.

[16] W. Su, et al., Phys. Chem. Chem. Phys. 21 (20) (2019) 10660.

[17] B. Jia, et al., Chem. Mater. 30 (1) (2018) 239.

[18] L. Chang, et al., Nanomaterials. 10 (9) (2020) 1759.

[19] Y. Luo, et al., Sol. RRL. 6 (12) (2022) 2200679.

[20] X. Du, et al., J. Mater. Chem. A. 7 (13) (2019) 7437.

[21] Y. Li, et al., Adv. Energy Mater. 11 (11) (2021) 2003408.

[22] Y. Cho, et al., ACS Appl. Energy Mater. 3 (8) (2020) 7689.

[23] Y. Wu, et al., Energy Environ. Sci. 12 (2) (2019) 675.

[24] M. Luo, et al., Mater. Chem. Front. 3 (11) (2019) 2483.

[25] J. Chen, et al., J. Mater. Chem. A. 7 (8) (2019) 3745.

[26] Y. Li, et al., J. Am. Chem. Soc. 139 (47) (2017) 17114.

[27] Y. Cui, et al., Adv. Mater. 29 (43) (2017) 1703080.

[28] T. Li, et al., Adv. Mater. 30 (10) (2018) 1705969.

[29] Y. Chang, et al., Nano Energy. 86 (2021) 106098.

[30] X. Huang, et al., Energy Environ. Sci. 15 (11) (2022) 4776.

[31] C. Y. Chang, et al., Adv. Funct. Mater. 23 (40) (2013) 5084.

[32] F. Liu, et al., Adv. Mater. 29 (21) (2017) 1606574.

[33] J. Zhang, et al., Adv. Mater. 31 (10) (2019) 1807159.

[34] P. Cheng, et al., Adv. Mater. 32 (39) (2020) 2003891.
[35] X. Duan, et al., Adv. Mater. 36 (18) (2024) 2308750.
[36] J. Yu, et al., Nat. Commun. 16 (2025) 7421.

## Figure captions

**Figure S1**. PL spectrum of various PM6 content in the L8-BO layer (The excitation wavelength is 266 nm).

**Figure S2.** Water contact angle images of the PM6, L8-BO, PM6/L8-BO, PM6/L8-BO:5 wt% PM6, PM6/L8-BO:10 wt% PM6, and PM6/L8-BO:15 wt% PM6 films.

**Figure S3.** (a) Device architecture of LBL opaque OSCs. (b) Energy levels diagrams used in this thesis; (c) Current density voltage (*J-V*) characteristics under AM 1.5 G solar irradiation (100 mW/cm$^2$) of PM6/L8-BO solar cells with different donor contents added in the L8-BO layer. Inset: *J-V* curves of the LBL opaque OSCs under dark. (e) $J_{ph}$-$V_{eff}$ plots of the LBL opaque OSCs devices.

**Figure S4.** AFM height and phase images of PM6 and L8-BO films.

**Figure S5.** (a) 2D GIWAXS patterns of PM6, L8-BO and PM6/L8-BO films with different PM6 content in the L8-BO layer. (b) Out-of plane (solid lines) and in-plane (dotted lines) of 1D GIWAXS for these active layer films.

**Figure S6.** (a) PM6 film thicknesses at different rotation speeds; (b) J-V characteristics of the devices with different PM6 film thicknesses.

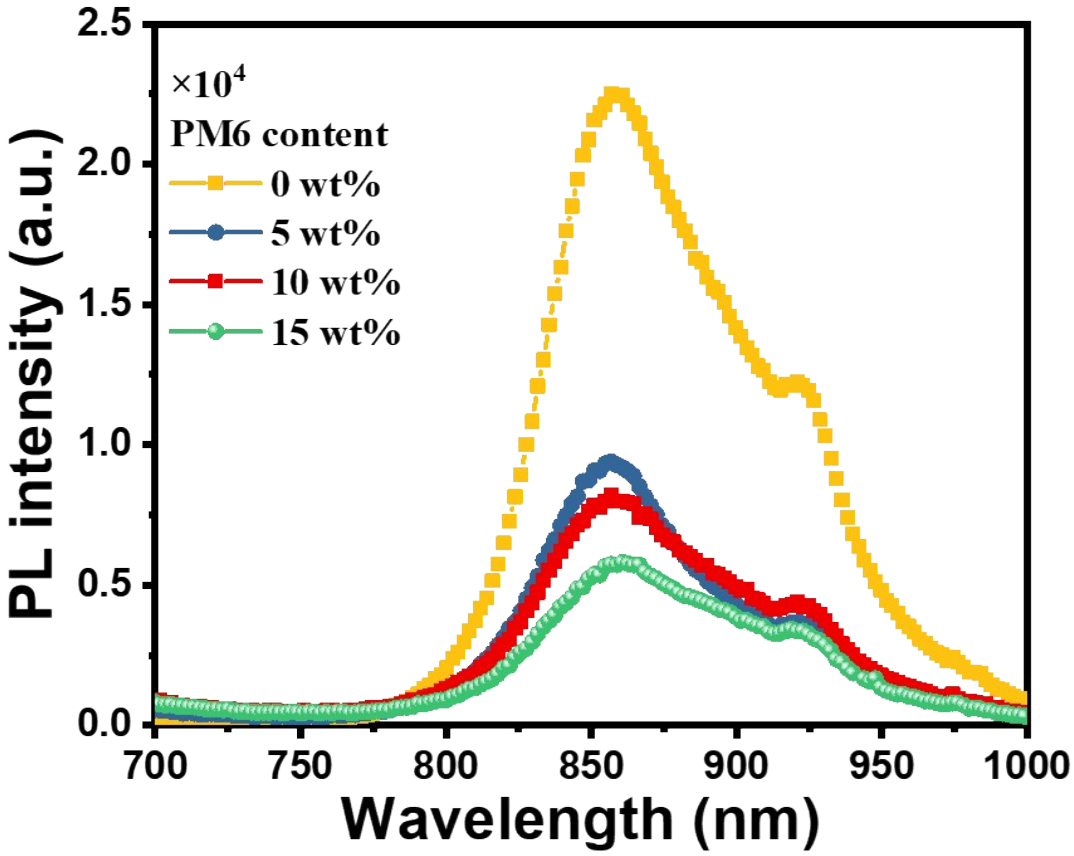
2.5
2.0
1.5
1.0
0.5
0.0
×10^4
PM6 content
0 wt%
5 wt%
10 wt%
15 wt%
PL intensity (a.u.)
700
750
800
850
900
950
1000
Wavelength (nm)

**Figure S1**

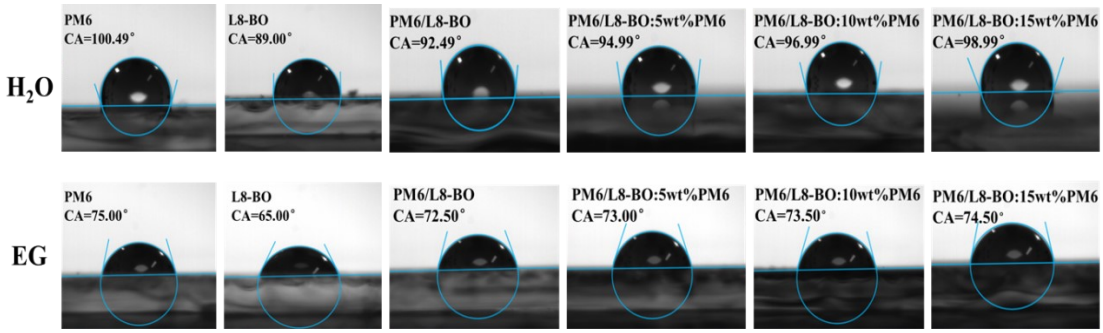
H2O
PM6
CA=100.49°
L8-BO
CA=89.00°
PM6/L8-BO
CA=92.49°
PM6/L8-BO:5wt%PM6
CA=94.99°
PM6/L8-BO:10wt%PM6
CA=96.99°
PM6/L8-BO:15wt%PM6
CA=98.99°
EG
PM6
CA=75.00°
L8-BO
CA=65.00°
PM6/L8-BO
CA=72.50°
PM6/L8-BO:5wt%PM6
CA=73.00°
PM6/L8-BO:10wt%PM6
CA=73.50°
PM6/L8-BO:15wt%PM6
CA=74.50°

**Figure S2**

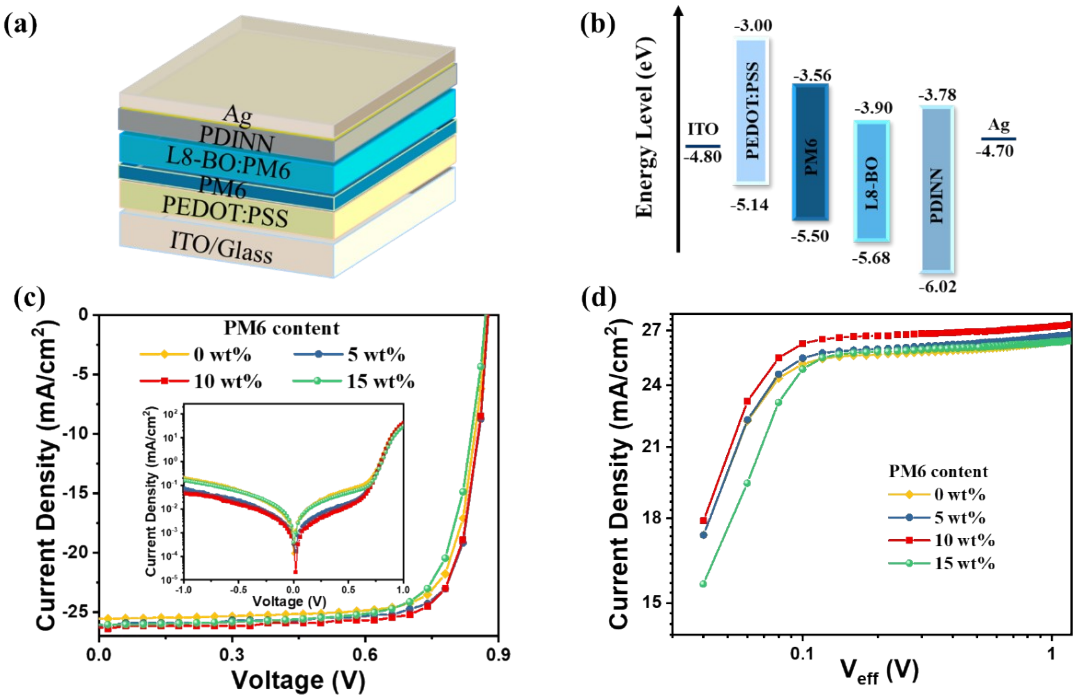
(a)
Ag
PDINN
L8-BO:PM6
PM6
PEDOT:PSS
ITO/Glass
(b)
Energy Level (eV)
ITO
-4.80
-3.00
PEDOT:PSS
-5.14
-3.56
PM6
-5.50
-3.90
L8-BO
-5.68
-3.78
PDINN
-6.02
Ag
-4.70
(c)
Current Density (mA/cm²)
Voltage (V)
PM6 content
0 wt%
5 wt%
10 wt%
15 wt%
(d)
Current Density (mA/cm²)
V_eff (V)
PM6 content
0 wt%
5 wt%
10 wt%
15 wt%

**Figure S3**

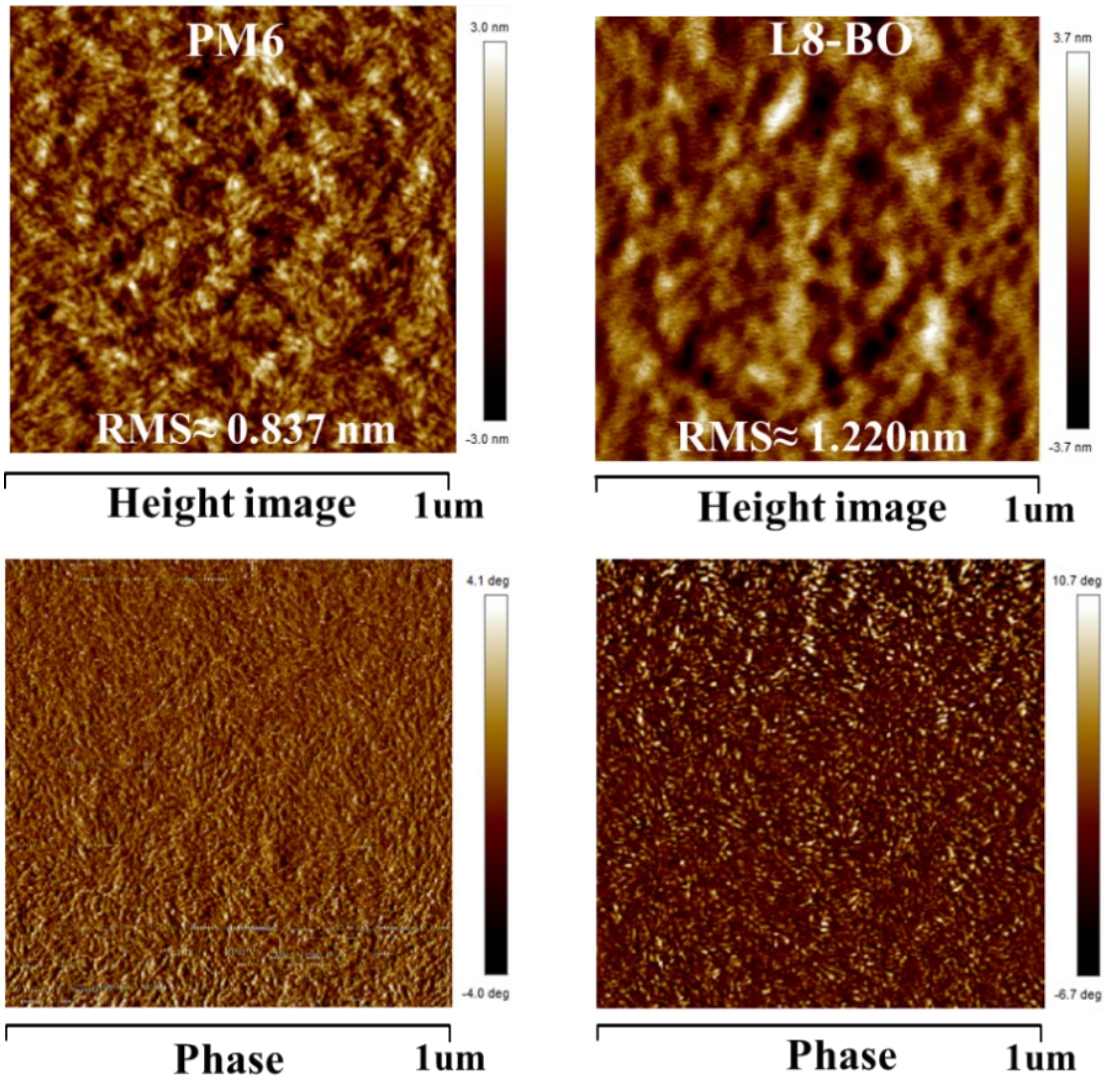
PM6
RMS≈ 0.837 nm
3.0 nm
-3.0 nm
Height image
1um
L8-BO
RMS≈ 1.220nm
3.7 nm
-3.7 nm
Height image
1um
4.1 deg
-4.0 deg
Phase
1um
10.7 deg
-6.7 deg
Phase
1um

**Figure S4**

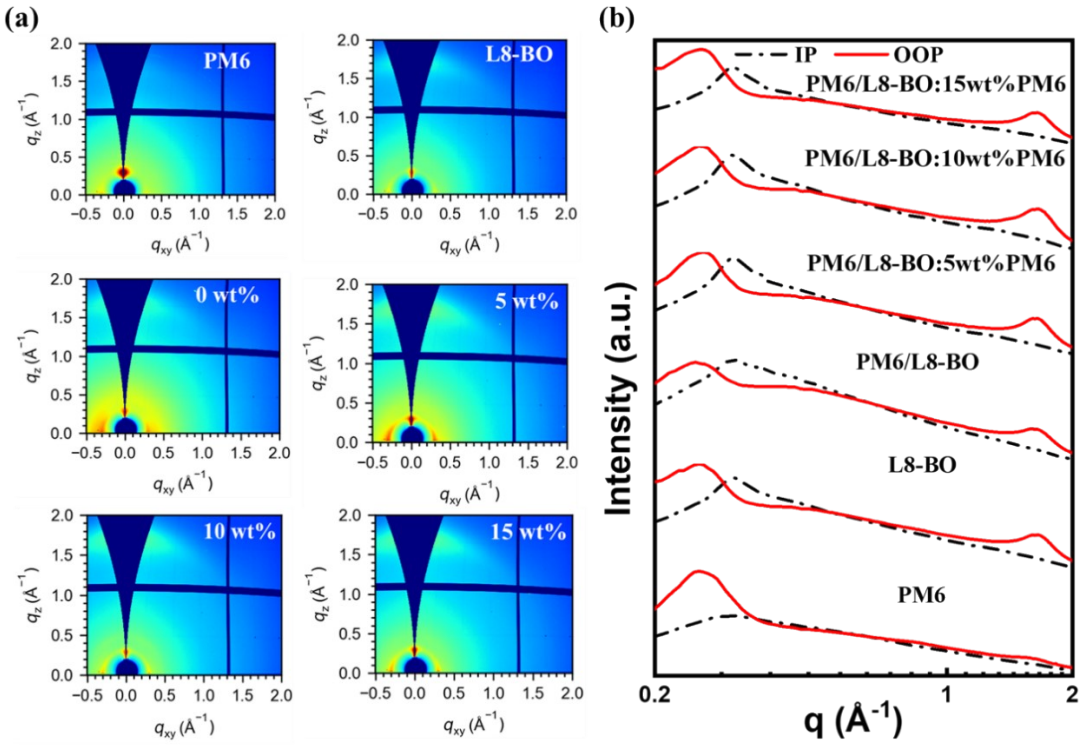
(a)
PM6
L8-BO
0 wt%
5 wt%
10 wt%
15 wt%
$q_z$ (Å$^{-1}$)
$q_{xy}$ (Å$^{-1}$)
(b)
IP
OOP
PM6/L8-BO:15wt%PM6
PM6/L8-BO:10wt%PM6
PM6/L8-BO:5wt%PM6
PM6/L8-BO
L8-BO
PM6
Intensity (a.u.)
q (Å$^{-1}$)

**Figure S5**

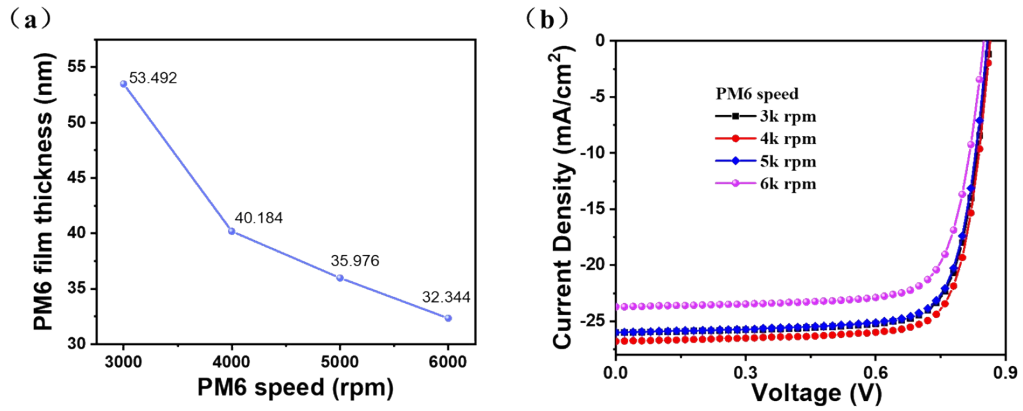
(a)
PM6 film thickness (nm)
55
50
45
40
35
30
53.492
40.184
35.976
32.344
3000
4000
5000
6000
PM6 speed (rpm)
(b)
Current Density (mA/cm$^2$)
0
-5
-10
-15
-20
-25
PM6 speed
3k rpm
4k rpm
5k rpm
6k rpm
0.0
0.3
0.6
0.9
Voltage (V)

**Figure S6**

**Table S1.** Detailed parameter base on binary system ST-OSC devices without complex optical engineering reported in the literature.

| Active layer | PCE (%) | AVT (%) | LUE (%) | Reference |
|---|---|---|---|---|
| PM6/L8-BO:5 wt% PM6 | 14.18 | 23.08 | 3.27 | This work |
| PM6/L8-BO:10 wt% PM6 | 15.26 | 20.43 | 3.12 | This work |
| PM6/L8-BO: 5wt% PM6 ($MoO_3$) | 12.98 | 27.65 | 3.58 | This work |
| PM6:Y6-BO (2PACz) | 15.2 | 19.2 | 2.91 | [1] |
| PM6:Y6 | 9.7 | 42.82 | 4.15 | [2] |
| PTB7-Th: ATT-9 | 9.37 | 35.5 | 3.33 | [3] |
| PM2: Y6-BO | 5.9 | 43.3 | 2.55 | [4] |
| PCE10-2Cl: IT-4F | 8.25 | 33 | 2.72 | [5] |
| PBT1-C-2Cl: Y6 | 9.1 | 40.1 | 3.65 | [6] |
| PCE10: A078 | 10.08 | 45.7 | 4.61 | [7] |
| PCE10-BDT2F:Y6 | 10.85 | 41.08 | 4.46 | [8] |
| PM6:Y6 | 12.37 | 18.6 | 2.3 | [9] |
| PTB7-Th/IEICO-4F | 8.8 | 40.9 | 3.6 | [10] |
| D18: N3 | 12.91 | 22.49 | 2.9 | [11] |
| PM6 (FPy=0.2): BTP-eC9 | 8.9 | 41.1 | 3.67 | [12] |
| PBDB-T-2F/Y6 | 12.22 | 25.5 | 3.12 | [13] |
| TAPC: Y6 | 3.01 | 47.99 | 1.44 | [14] |
| 66-PTB: IEICO-4F | 5.11 | 50.82 | 2.6 | [15] |
| PBFTT: IT-4Cl | 9.1 | 27.6 | 2.51 | [16] |
| PTB7-Th: IUIC | 10.3 | 31 | 3.16 | [17] |
| PM6:N3 | 9.18 | 28.94 | 2.66 | [18] |
| DEH-20: L8-BO | 14.6 | 22 | 3.29 | [19] |
| PTB7-Th: PC71BM | 12.41 | 25.33 | 3.14 | [20] |
| PTB7-Th:H3 | 8.38 | 50.09 | 4.2 | [21] |
| DTG-IW: PTB7-Th | 6.19 | 50.4 | 3.12 | [22] |
| PBN-S: IT-4F | 9.83 | 32 | 3.15 | [23] |
| PBDB-T: Y14 | 12.67 | 23.69 | 3 | [24] |
| PTB7-Th: ACS8 | 11.1 | 28.6 | 3.17 | [25] |
| PCE-10: BT-CIC | 7.1 | 43 | 3.05 | [26] |
| PTB7-Th: IEICO-4Cl | 8.38 | 25.7 | 2.15 | [27] |
| PTB7-Th: FOIC | 10.3 | 37.4 | 3.85 | [28] |
| PL-Cl: F8IC | 11 | 35 | 3.85 | [29] |
| PCE10-2F/Y6 | 10 | 50.5 | 5.01 | [30] |
| PCPDTFBT: PC71BM | 5.0 | 47 | 2.35 | [31] |
| PTB7-Th: ATT-2 | 7.7 | 37 | 2.85 | [32] |
| J71: IHIC | 8.3 | 28 | 3.32 | [33] |

| | | | | |
|---|---|---|---|---|
| PBDB-T: Y1 | 10.9 | 20 | 2.18 | [34] |
| PP2+DB/BTP-eC9+DB | 11 | 42.98 | 4.77 | [35] |
| PBOF: eC9: PC61BM | 12.9 | 49.2 | 6.05 | [36] |

**Table S2.** Photovoltaic parameters of LBL opaque OSCs with different donor contents added in the L8-BO layer

| PM6 (wt%) | $V_{OC}$ (V) | $J_{SC}$ (mA/cm$^2$) | FF (%) | PCE (Ave. ±Dev)[a)] (%) |
|---|---|---|---|---|
| 0 | 0.874 | 25.55 | 77.93 | 17.41(17.29±0.13) |
| 5 | 0.878 | 26.03 | 79.38 | 18.13(17.98±0.21) |
| 10 | 0.877 | 26.25 | 79.04 | 18.21(18.11±0.16) |
| 15 | 0.872 | 26.05 | 75.02 | 17.04(16.94±0.18) |

a) All values in parenthesis are average photovoltaic values from 10 devices.

**Table S3.** Summary of $P_{coll}$, $P_{diss}$ values of LBL opaque OSCs with different PM6 dispersant added in the L8-BO layer

| PM6 (wt%) | 0 | 5 | 10 | 15 |
|---|---|---|---|---|
| $P_{coll}$ | 86.88 | 88.93 | 88.96 | 88.86 |
| $P_{diss}$ | 95.96 | 97.02 | 97.51 | 97.30 |

**Table S4.** Summary of the $d_{\text{-spacing}}$ and crystal coherence length of the films with PM6, L8-BO and various PM6 content in the L8-BO layer.

| film | $q_{xy}$ (Å$^{-1}$) | $d_{\text{-spacing}}$[a)] (Å) | FWHM[b)] (Å$^{-1}$) | $CCL_{010}$ (Å) | $q_z$ (Å$^{-1}$) | $d_{\text{-spacing}}$[a)] (Å$^{-1}$) | FWHM[b)] (Å$^{-1}$) | $CCL_{010}$ (Å) |
|---|---|---|---|---|---|---|---|---|
| PM6 | 0.30 | 20.93 | 0.54 | 10.35 | 1.56 | 4.03 | 0.82 | 6.82 |
| L8-BO | 0.31 | 20.26 | 0.22 | 25.41 | 1.66 | 3.78 | 0.48 | 11.64 |
| PM6/L8-BO | 0.31 | 20.26 | 0.37 | 15.11 | 1.65 | 3.81 | 0.50 | 11.18 |
| PM6/L8-BO: 5 wt% PM6 | 0.31 | 20.26 | 0.16 | 34.93 | 1.65 | 3.81 | 0.46 | 12.15 |
| PM6/L8-BO: 10 wt% PM6 | 0.31 | 20.26 | 0.18 | 31.05 | 1.65 | 3.81 | 0.45 | 12.42 |
| PM6/L8-BO: 15 wt% PM6 | 0.31 | 20.26 | 0.20 | 27.95 | 1.65 | 3.81 | 0.45 | 12.42 |

a) The $d_{\text{-spacing}}$ of molecular stacking can be calculated by the equation $d_{\text{-spacing}} = \frac{2\pi}{q_z}$.

b) The crystallinity coherent lengths ($CCL$) are evaluated according to the equation: $CCL = \frac{2\pi k}{FWHM}$, where $k$ is the shape factor, typically with the value of 0.89, and FWHM is related to the full-width at half-maximum.

**Table S5.** Summary of $V_{OC}$, $J_{SC}$, FF and PCE of the opaque devices with different PM6 thickness layer.

| PM6 speed (rpm) | $V_{OC}$ (V) | $J_{SC}$ (mA/cm$^2$) | FF (%) | PCE (%) |
|---|---|---|---|---|
| 3000 | 0.862 | 25.50 | 77.19 | 16.96 |
| 4000 | 0.864 | 26.24 | 77.98 | 17.69 |
| 5000 | 0.857 | 25.48 | 77.12 | 16.83 |
| 6000 | 0.850 | 23.24 | 76.07 | 15.02 |